Available online at www.sciencedirect.com
SCIENCE DIRECT®
Journal of Nuclear Materials 340 (2005) 179–186
journal of nuclear materials
www.elsevier.com/locate/jnucmat

Environment and oxidation state of molybdenum in simulated high level nuclear waste glass compositions

R.J. Short *, R.J. Hand, N.C. Hyatt, G. Möbus

Immobilisation Science Laboratory, Department of Engineering Materials, University of Sheffield, Sir Robert Hadfield Building, Mappin Street, Sheffield S1 3JD, UK

Received 23 July 2004; accepted 18 November 2004

Abstract

Alkali borosilicate glasses containing between 20 and 35 wt% of a simulated high level nuclear waste stream with varying Li_2O contents were melted under neutral (air) and reducing (nitrogen/hydrogen) conditions. XRD analysis of the as-cast glasses showed a tendency for the products to remain amorphous when melted under neutral conditions and for metallic silver to develop in the reduced melts. EXAFS analysis revealed $(MoO_4)^{2-}$ tetrahedra in all glasses regardless of the sparge applied during melting. The glasses were heat treated to simulate an interruption to the cooling system used to prevent heat build-up in the vitrified product store. Powellite-type molybdate phases were found to develop in the heat treated samples and formed at lower waste loadings in glasses sparged with a reducing gas. A reduction in the quantity of Li_2O lead to a reduction in the quantity of powellite-type molybdate phases. EDS showed the primary molybdate phase to be high in Sr and rare earth elements and TEM indicated that the presence of silver metal encouraged molybdate formation.

1. Introduction

Alkali borosilicate glasses are used as vitrification matrices for high level nuclear waste (HLW) due to their good waste incorporation and chemical durability properties along with their relative low cost and ease of manufacture [1,2]. One problem with alkali borosilicates is that Mo, an element found in high concentrations in many HLW streams, has a low solubility in these compositions. At levels greater than 1% [3], Mo tends to combine with other elements from the HLW to form a mixture of alkali molybdates (along with chromates and sulphates) generally termed 'yellow phase' due to its colour. In the liquid state, yellow phase enhances the corrosion of inconel crucible liners in HLW vitrification plants and in the solid state it can be water soluble, which could lead to increased leaching of radionuclei from the vitrified waste should it ever come into contact with water. Thus, for HLW streams high in Mo, waste loadings in the borosilicate network have to be restricted to prevent yellow phase formation.

It has previously been suggested that lowering the oxidation state of Mo in the melt could lead to a greater solubility in the borosilicate matrix and prevent the formation of yellow phase [3]. To investigate this theory, alkali borosilicate batches containing a simulated HLW stream at waste loadings of 20, 25, 30 and 35 wt% were

* Corresponding author. Tel.: +44 114 222 5973.
E-mail address: r.j.short@sheffield.ac.uk (R.J. Short).

0022-3115/$ - see front matter © 2004 Elsevier B.V. All rights reserved.
doi:10.1016/j.jnucmat.2004.11.008

sparged with compressed air and a reducing composition of nitrogen/5% hydrogen during melting. The glasses were analyzed in the as-cast state and then heat treated (to simulate an interruption to the cooling system used to prevent heat build-up in the vitrified product store) and further analyzed to determine the oxidation state and environment of the Mo. Previous analysis of yellow phase from full scale simulated HLW melts has identified $LiCsMoO_4$ as one of the primary components of the compound [4], and thus glasses with 35 wt% waste loadings and reduced Li_2O contents were also melted in order to investigate whether reducing the Li_2O content affected molybdate formation.

2. Experimental procedure

The compositions of the batches used in these experiments are shown in Table 1. The glass 1 base composition (i.e. the SiO_2, B_2O_3, Na_2O and Li_2O levels) is representative of the MW glass frit composition used in the active Waste Vitrification Plant at Sellafield, and for glasses 2–4 (with higher waste loadings) the proportions of constituents in the base glass have been kept constant relative to one another. In glasses 5–8, the waste loading is kept constant at 35 wt% and the quantity of Li_2O in the base glass is progressively reduced, and balanced by proportional increases in the SiO_2, B_2O_3 and Na_2O ratios. The simulated HLW waste stream used in this work represents a stream that is based on the projected fission products of a 4:1 blend of high burn up (HBU) UO_2 fuel and mixed oxide (MO_x) fuel, a hypothetical future fuel cycle scenario. To avoid the use of radioactive isotopes and to reduce costs, rare earth elements such as Pr and Eu have been simulated by increasing the amount of Nd_2O_3, and AgO has been used to represent Rh, Pd and Cd oxides. TiO_2 was used to model TcO_2. The high proportion of Mo in the waste stream is due to its use as a fuel additive and the Gd_2O_3 has been added as a neutron poison, not a fission product. The oxide form of the elements used for this simulated waste stream may not be 100% representative of the oxidation states of active HLW elements; a certain proportion of these elements would be present as nitrates (Sr, Cs and La, for example) or metals (such as Rh and Pd) upon introduction to the melting furnace. Ru was omitted from the simulated HLW stream due to cost.

Table 1
Glass compositions

Glass	1[a]	2[a]	3[a]	4[a]	5	6	7	8
Wt% waste	20	25	30	35	35	35	35	35
Oxide	Wt (g)	Wt (g)	Wt (g)	Wt (g)	Wt (g)	Wt (g)	Wt (g)	Wt (g)
SiO_2	50.19	47.23	44.25	41.25	41.25	41.82	42.40	43.56
B_2O_3	17.79	16.74	15.68	14.62	14.62	14.82	15.03	15.43
Na_2O	8.93	8.41	7.88	7.34	7.34	7.44	7.55	7.75
Li_2O	4.30	4.05	3.80	3.54	3.54	2.65	1.77	0.00
Ag_2O	1.43	1.80	2.16	2.53	2.53	2.53	2.53	2.53
BaO	0.95	1.19	1.44	1.68	1.68	1.68	1.68	1.68
CeO	1.35	1.69	2.04	2.39	2.39	2.39	2.39	2.39
Cs_2O	1.33	1.67	2.01	2.35	2.35	2.35	2.35	2.35
Gd_2O_3	2.82	3.53	4.26	4.99	4.99	4.99	4.99	4.99
La_2O_3	0.72	0.90	1.09	1.28	1.28	1.28	1.28	1.28
MoO_3	2.43	3.05	3.67	4.30	4.30	4.30	4.30	4.30
Nd_2O_3	3.04	3.82	4.60	5.38	5.38	5.38	5.38	5.38
Rb_2O	0.17	0.21	0.25	0.29	0.29	0.29	0.29	0.29
Sm_2O_3	0.45	0.56	0.68	0.79	0.79	0.79	0.79	0.79
SrO	0.42	0.53	0.64	0.74	0.74	0.74	0.74	0.74
TeO_2	0.12	0.15	0.18	0.22	0.22	0.22	0.22	0.22
TiO_2	0.54	0.68	0.82	0.96	0.96	0.96	0.96	0.96
Y_2O_3	0.25	0.31	0.38	0.44	0.44	0.44	0.44	0.44
ZrO_2	2.24	2.81	3.38	3.96	3.96	3.96	3.96	3.96
Fe_2O_3	0.34	0.42	0.51	0.60	0.60	0.60	0.60	0.60
NiO	0.10	0.12	0.14	0.17	0.17	0.17	0.17	0.17
Cr_2O_3	0.10	0.13	0.15	0.18	0.18	0.18	0.18	0.18
Total	100.00	100.00	100.00	100.00	100.00	100.00	100.00	100.00

[a] The suffixes 'air' and 'red' are used in the main text to denote glasses sparged with compressed air and nitrogen/5% hydrogen gases respectively during melting.

The necessary chemicals for a given composition were weighed to an accuracy of ±0.005 g and placed in a stainless steel vessel. They were then intimately mixed using a PVC spatula, transferred to an alumina crucible and preheated to 1000 °C at 1 K/min. The glasses were then placed into an electric melting furnace at 1150 °C and given a residence time of 1 h. This furnace temperature was increased to 1175 °C, 1200 °C and 1300 °C for glasses 6, 7 and 8 respectively to allow for the increased viscosity of these glasses caused by the decrease in Li content. For glasses 1–4, an alumina tube connected to the appropriate gas cylinder (containing compressed air or nitrogen/5% hydrogen) was then inserted into the melt to a depth of approximately 10 mm above the base of the crucible, and the melt was sparged (with gas flow rates of ~3.5 l/min) for 4.5 h. For glasses 5–8, an alumina stirring paddle was inserted into the melt to a depth of approximately 10 mm above the base of crucible and was then rotated at 60 rpm for 4.5 h. The glasses were then poured into a preheated steel block mould and annealed at 550 °C for 1 h and cooled to room temperature at 1 K/min. For heat treatment, cubes of approximately $10 \times 10 \times 10$ mm were cut from the as-cast blocks using a diamond saw. These were placed in an alumina boat crucible and held for 48 h at 600 °C in air, with heating and cooling rates of 5 °C/min. Henceforth, glasses sparged with compressed air will be denoted glass #(air), and those sparged with nitrogen/hydrogen as glass #(red).

XRD was performed using a Philips PW1373 X-ray Powder Diffractometer. Samples were ground to a fine enough size for diffraction (<200 μm) using an agate mortar and pestle, front loaded into an aluminium sample tray, and scanned using Cu Kα or Co Kα radiation at 50 kV. The step size used was 0.02°, and the scanning speed was nominally 0.5°/min over a range of 10–60°2θ (for Cu kα radiation) or 15–80°2θ (for Co kα radiation). The patterns obtained were matched to the ICDD files using the Stoe X-ray diffraction computer analysis software WinXPOW. Some of the samples were ground and sieved to ⩽75 μm and re-scanned to check for particles size effects. No significant differences between the scans could be observed. For ease of comparison, the Co traces have been converted to Cu traces using the formula:

$$2\theta_2 = 2\{\sin^{-1}(\lambda_2/\lambda_1 \cdot \sin[2\theta_1/2])\},$$

where $2\theta_1$ and λ_1 are the original Co diffraction angles and Co K_α wavelength, and $2\theta_2$ and λ_2 are the Cu diffraction angles and Cu K_α wavelength. The values used for the wavelengths were 1.78896 Å and 1.54060 Å for Co and Cu respectively. Due to a slight overlap of the sample holder into the X-ray beam path on the diffractometer fitted with the Co source, reflections of Al metal were present on all traces obtained using this equipment. In order to confirm that these reflections were artifacts due to the equipment, several of the samples were re-scanned using the Cu source diffractometer and no Al reflections were observed.

TEM analysis was performed using a Jeol JEM-2010F Field Emission Gun TEM. The samples were prepared by polishing on both sides alternately using 120, 240, 600 and 1200 grit papers until they were approximately 30 μm in thickness. They were then cleaned using acetone, broken into small pieces approximately 3 mm across, and glued using epoxy resin to a 3.05 mm diameter copper ring with a 1 mm diameter hole in the middle. The samples were then further thinned using a Gatan ion beam miller until perforation gave a small hole in the center of the disc surrounded by thin (~20–50 nm) area. They were then carbon coated before being viewed in the microscope. An accelerating voltage of 200 kV was used, and a Gatan Digiscan imager was used to acquire STEM images of samples using an Annular Dark Field (ADF) detector which generates Z-contrast, inverted in comparison to standard bright-field STEM images. An Oxford Link Isis EDS system was used to acquire EDS analysis from some samples.

Mo K-edge X-ray absorption spectra were collected on Station 16.5 at the Synchrotron Radiation Source, Daresbury, UK. The storage ring operates at 2 GeV with a typical beam current of 150 mA. A double crystal Si(220) monochromator was used detuned to 50% of maximum intensity for harmonic rejection. The Mo K absorption edge was calibrated by measuring the K-edge from a Mo foil at 20005 eV. Spectra were recorded at ambient temperature in transmission mode using ion chambers filled with a mixture of Ar (698 mbar)/balance He (incident beam, I_0) and Kr 368 mbar/balance He (transmitted beam, I_t). The samples, in the form of fine powders, diluted where necessary with BN (in a ca. 1:10 volume ratio), were packed into aluminium sample holders. At least two data sets were acquired per sample, over the energy range 19850–20850 eV. The spectral data were summed, calibrated and background subtracted using the programs EXCALIB, EXSPLINE and EXBACK. The background subtracted EXAFS data were analyzed using EXCURV98. Theoretical fits were obtained by adding shells of backscattering atoms around the central absorber atom (Mo) and refining the Fermi energy, E_f, the absorber–scatterer distances, r and the Debye-Waller factors, $2\sigma^2$, in order to minimize the sum of the squares of the residuals between the experiment and the theoretical fit. Shell occupancies were fixed at the integral values which gave the best fit as indicated by the EXAFS goodness of fit parameter, or R-factor, as calculated by EXCURV98. The estimated precision in the refined absorber–scatterer contact distances is ±0.02 Å, the relative precision in the refined Debye Waller parameters is estimated to be ±25%.

3. Results and discussion

3.1. As-cast glasses

XRD data for the as-cast air sparged glasses (Fig. 1) shows that all of the glasses remained amorphous to XRD. However, reflections at 38.2°2θ and 44.4°2θ with d-spacings of 0.2354 nm and 0.204 nm in the data for the reduced as-cast glasses (Fig. 2) had a good match with card [4-783] from the ICDD database, showing that even at the lowest (20 wt%) waste loading devitrification of metallic silver occurred under reducing conditions. One can infer from this that in an active HLW composition, devitrification of the dissolved fraction of elements such as Rh and Pd (for which Ag is used as a simulant in this work) would be very likely if a reducing sparge was applied to the glass during melting. As these elements are likely to be denser than the glass melt (which is usually of the order of 2.9 g cm^{-3}), they would worsen the problem of heel formation. A heel is a dense layer of heavy metals and metallic oxides, immiscible with the melt, which forms in the bottom of the melting vessel and eventually blocks the pouring spout of the melter, requiring a time consuming unplugging procedure and sometimes necessitating a costly replacement. However, as a significant proportion of the 4d elements in a real HLW would be present as undissolved metals upon introduction to the melting vessel, the reduction of the dissolved fraction should not have a major effect on the problem of heel formation. Mo K-edge EXAFS analysis of the as-cast glasses 1(air), 1(red), 4(air) and 4(red) (Figs. 3(a)–(d) and 4(a)–(d) and Table 2) show that only one coordination shell was present around the molybdenum in all glasses at a distance of 1.76(2) Å. This had a good fit with a model of four oxygens in tetrahedral coordination around the Mo centers. It can also be inferred from the lack of a second coordination shell that the charge balancing of the $[MoO_4]^{2-}$ tetrahedra is carried out by a random distribution of cations in the silicate network, and that the $[MoO_4]^{2-}$ tetrahedra take up network modifier positions in the

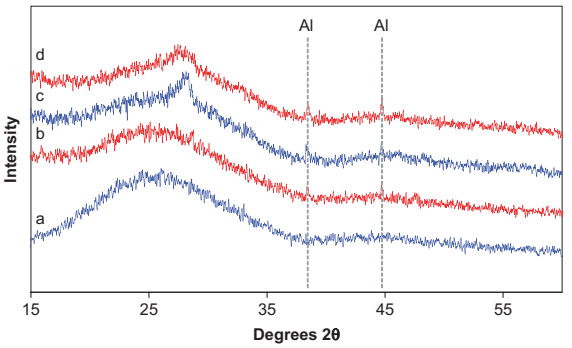

Fig. 1. XRD of as-cast samples of (a) glass 1(air), (b) glass 2(air), (c) glass 3(air), (d) glass 4(air). Reflections from the aluminium sample holder are labeled 'Al'.

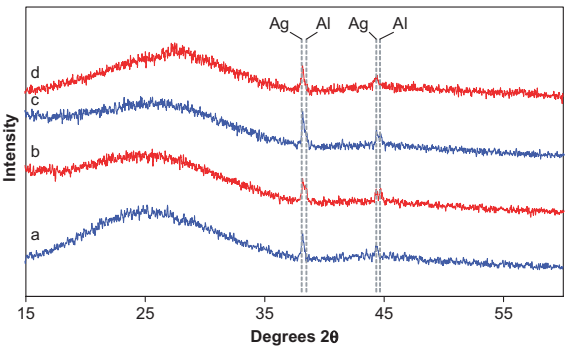

Fig. 2. XRD of as-cast samples of (a) glass 1(red), (b) glass 2(red), (c) glass 3(red), (d) glass 4(red). Reflections from the aluminium sample holder are labeled 'Al', and reflections from silver metal are labeled 'Ag'.

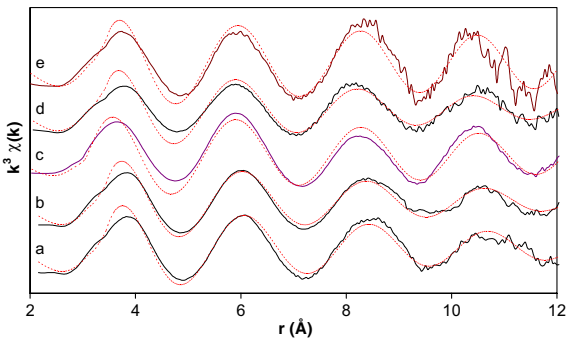

Fig. 3. Background subtracted EXAFS of (a) as-cast glass 1(air), (b) as-cast glass 1(red), (c) as-cast glass 4(air), (d) as-cast glass 4(red), (e) heat treated glass 4(red).

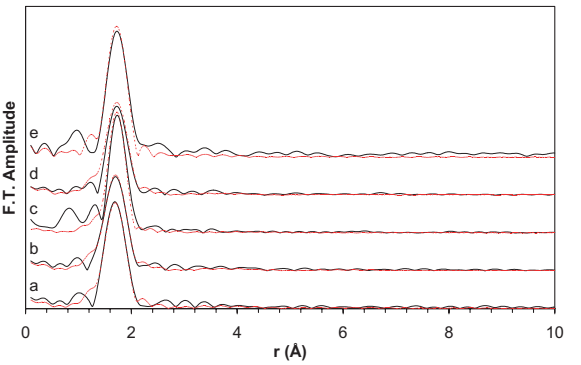

Fig. 4. Fourier transforms of EXAFS results of (a) as-cast glass 1(air), (b) as-cast glass 1(red), (c) as-cast glass 4(air), (d) as-cast glass 4(red), (e) heat treated glass 4(red).

Table 2
Summary of model parameters used for EXAFS curve fitting

Sample	Shell	Type	Occupancy	r (Å)	R
Glass 1(air) as-cast	1	O	4	1.76	24.5
Glass 1(red) as-cast	1	O	4	1.76	21.8
Glass 4(air) as-cast	1	O	4	1.76	19.0
Glass 4(red) as-cast	1	O	4	1.76	34.0
Glass 4(red) heat treated	1	O	4	1.76	33.7

'r' is the distance to the central Mo atom, 'R' is the goodness of fit.

matrix and are not bonded to the borosilicate framework. This is in good agreement with the work of Calas et al. [5] who performed similar EXAFS experiments on some French SON68 simulated HLW glass compositions. Calas et al. also used computer simulations of simplified HLW glass networks to show that $[MoO_4]^{2-}$ tetrahedra are likely to exist in alkali and alkaline earth rich sublattices in the borosilicate matrix.

Some of the stirred glasses exhibited differences to the 35 wt% waste loaded sparged glasses in that non-metallic crystalline phases developed in glasses 5 and 8 (see Fig. 5). The single crystalline reflection in the XRD of glass 5 was not sufficient to make a positive identification of the phase, however the multiple reflections (of which the three major d-spacings were 0.322 nm, 0.270 nm and 0.199 nm, labeled '♦' in Fig. 5(d)) seen in glass 8 did closely resemble some of the patterns contained in the ICDD database which were all powellite-type molybdate phases, e.g. $NaLa(MoO_4)_2$ (card [79-2243]). The powellite mineral $CaMoO_4$ is a tetragonal mineral with the scheelite structure (Space group $I4_1/a$), and is capable of incorporating a wide range of mono, di and trivalent cations on the Ca site (see, for example Shi et al. [6] and Schieber and Holmes [7]). Thus it is likely that several of the elements of the simulated HLW present in this composition were incorporated in the powellite type phase seen in glass 8, producing a molybdate with a composition that has not previously been synthesized or characterized in the ICDD database, and therefore could not be exactly matched. Whilst a small quantity (<1%) of crystalline material (as seen in the as-cast glass 5) can be tolerated in real HLW glasses, the presence of significant quantities of crystalline material in the as-cast state would be undesirable in a real HLW glass and thus the XRD of glass 8 indicated that a complete absence of Li in the batch would have a negative effect on the quality of the product.

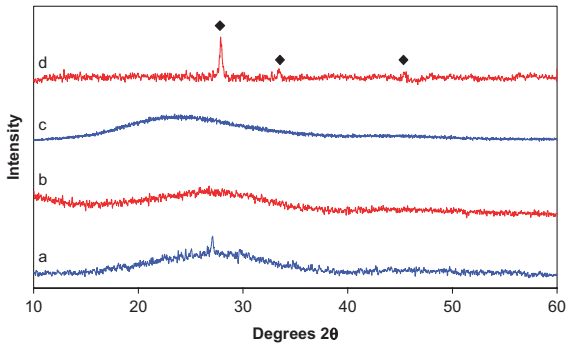

Fig. 5. XRD of as-cast samples of (a) glass 5, (b) glass 6 (c) glass 7 (d) glass 8. N.B. The background has been subtracted from (d) to highlight the crystalline reflections.

3.2. Heat treated glasses

XRD of the heat treated air sparged glasses (Fig. 6) shows that at waste loadings $\geqslant$25 wt%, a crystalline phase developed during heat treatment (labeled '▼' in Fig. 6) with d-spacings of the three most intense reflections of 0.316 nm, 0.265 nm and 0.197 nm (at 28.56°2θ, 30.47°2θ and 46.09°2θ respectively). Although no exact match for the phase could be found using the International Centre for Diffraction Data (ICDD) database, several close matches were found for powellite-type molybdate phases such as $AgNd(MoO_4)_2$ (card [49-380]), $Nd_2(MoO_4)_3$ (card [73-1212]) and $NaCe(MoO_4)_2$ (card [79-2242]). Reflections at 38.2°2θ and 44.4°2θ also indicated the presence of silver in the heat treated glass 4(air) sample via a match with card [4-783] from the ICDD database, but this metallic phase was not seen in any of the other air sparged glass samples. STEM and EDS analysis of a heat treated glass 4(air) sample revealed the presence of both needle-like and circular (which were possibly cross sectioned needle-like particles) crystalline molybdate phases, seen as light grey particles against the dark grey amorphous matrix in Fig. 7 and labeled 'Mo Needle' and 'Mo' respectively. The

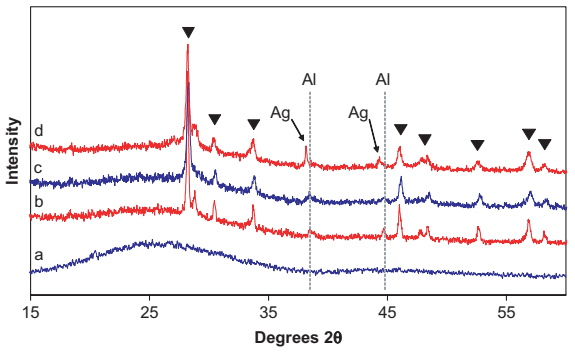

Fig. 6. XRD of heat treated samples of (a) glass 1(air), (b) glass 2(air), (c) glass (air), (d) glass 4(air). Reflections from Ag metal in (d) and the Al sample holder in (c) and (d) are labeled – all other reflections originate from the powellite-type molybdate phase present in (b), (c) and (d).

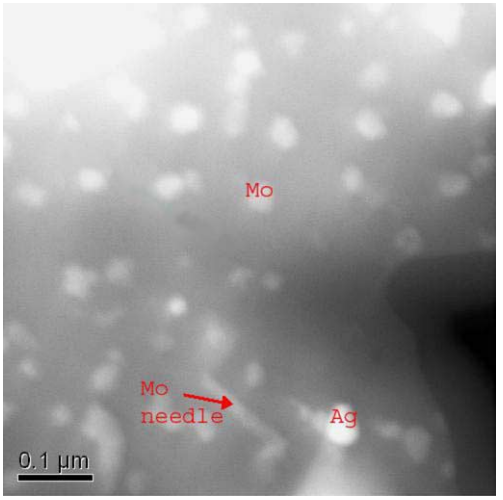

Fig. 7. STEM ADF image of a heat treated sample of glass 4(air). The brightest particles are metallic silver (labeled 'Ag') and light grey molybdate particles high in Sr and lanthanide elements (labeled 'Mo' and 'Mo needle') can be seen against the darker grey alkali borosilicate matrix.

analysis also revealed the presence of metallic silver which can be seen as white particles and labeled 'Ag' in Fig. 7. The molybdate particles were shown by EDS to be higher in Sr and lanthanide elements than the surrounding matrix. This would have important implications in a real HLW glass, as ^{90}Sr is responsible for a significant proportion of the emitted radiation for the first few hundred years of the existence of the waste, and thus it is important that this element does not become incorporated in a phase of potentially lower durability than the glass matrix.

XRD of the heat treated glasses sparged with a reducing gas (Fig. 8) showed that at all waste loadings

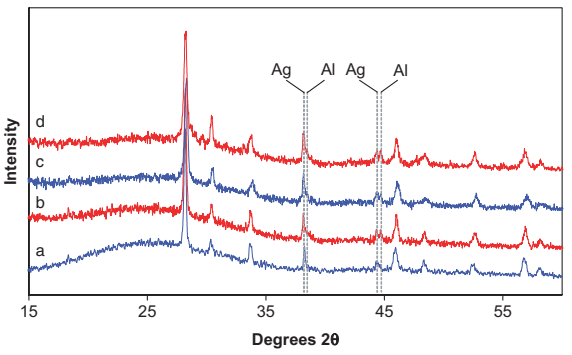

Fig. 8. XRD of heat treated samples of (a) glass 1(red), (b) glass 2(red), (c) glass (red), (d) glass 4(red). Reflections from Ag metal and the Al sample holder are labeled – all other reflections originate from the powellite-type molybdate phase present in (b), (c) and (d).

a crystalline phase with major *d*-spacings of 0.316 nm, 0.265 nm and 0.197 nm developed. These reflections are in the same positions as those of the powellite-type molybdate phase observed in the air sparged glasses loaded with $\geqslant$25 wt% waste. STEM imaging of a sample of heat treated glass 1(red) (Fig. 9(a)) revealed the presence of dendritic molybdate particles that, as for the heat treated glass 4(air) samples, were shown to be high in Sr and lanthanides. Wider analysis of this sample (Fig. 9(b)) revealed a trend for the densest clusters of molybdate particles to be located close to particles of silver, indicating that silver particles may encourage the formation of the molybdate phase. Whilst the real HLW composition would contain much lower quantities of silver than are present in this glass, the heavy metals for which silver acts as an analogue have been well documented as being prone to devitrification during melting even under oxidizing conditions (see, for example [2,3]) and thus could encourage molybdate formation in real HLW systems. STEM imaging (Fig. 10) and EDS analysis of a heat treated glass 4(red) sample again showed the presence of molybdate particles (labeled 'Mo' in Fig. 10) high in Sr and lanthanides. Mo K-edge EXAFS analysis of this sample (Figs. 3(e), 4(e) and Table 2) revealed only the presence of $[MoO_4]^{2-}$ tetrahedra. The lack of a second coordination shell again indicated that the distribution of the $[MoO_4]^{2-}$ charge balancing cations (i.e. the Sr and lanthanide elements) in the powellite-type molybdate phase is random.

The heat treated samples of glasses 5–8 demonstrated a different pattern of crystallization to glasses 4(air) and 4(red) which contained the same (35 wt%) waste loading. The XRD of the heat treated glass 5 (Fig. 11(a)) sample showed that two distinct powellite-type molybdate phases were present. The phase causing the reflections at 27.08°2θ, 32.62°2θ and 45.60°2θ with *d*-spacings of 0.329 nm, 0.274 nm and 0.199 nm (labeled 'W' in Fig. 11(a)) may already have been present in the as-cast glass, as there is a reflection with a *d*-spacing of 0.329 nm on the XRD of the as-cast glass 5 (Fig. 11(a)). The second phase present in the heat treated glass 5 sample could be seen as reflections at 27.94°2θ, 33.50°2θ and 46.02°2θ with *d*-spacings of 0.319 nm, 0.267 nm and 0.197 nm (labeled 'X' in Fig. 11(a)). These values were very similar to the crystalline reflections seen in the heat treated glasses 1–4 samples, indicating that they may have been caused by the same powellite-type molybdate phase. In the heat treated glass 6 sample (containing only 3/4 the quantity of Li_2O present in glasses 4 and 5), a different crystalline phase to either of those seen in the heat treated glass 5 was present, as indicated by reflections at 27.70°2θ, 33.20°2θ and 45.58°2θ with *d*-spacings of 0.322 nm, 0.270 nm and 1.99 nm respectively (labeled 'Y' in Fig. 11(b)). This phase was the same as that seen in the as-cast glass 8 sample (Fig. 11d). Another reflection was also present in the heat treated glass 6 sample (labeled

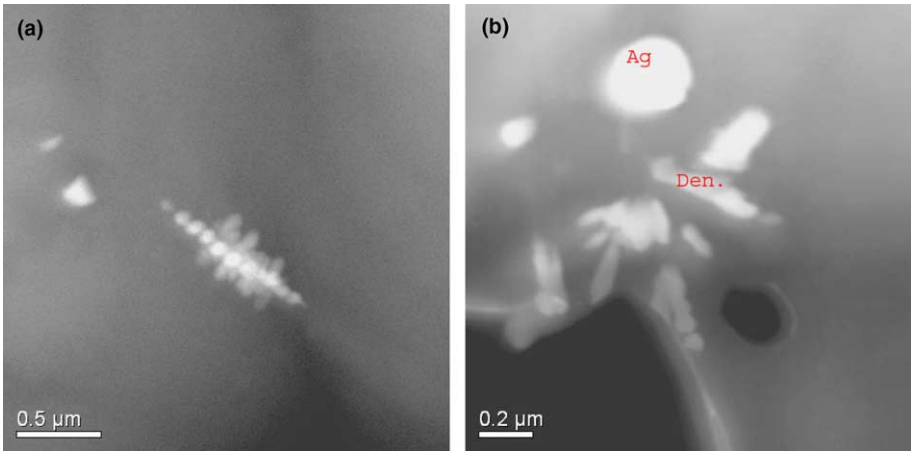

Fig. 9. STEM ADF image of a heat treated sample of glass 1(red): (a) showing a dendritic powellite-type molybdate particle high in Sr and lanthanides and (b) showing molybdate dendrites in close proximity to Ag particles.

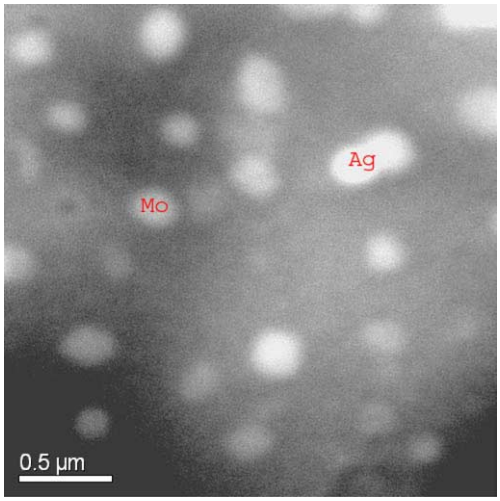

Fig. 10. STEM ADF image of a heat treated sample of glass 4(red) showing powellite type molybdate and Ag particles in the borosilicate matrix.

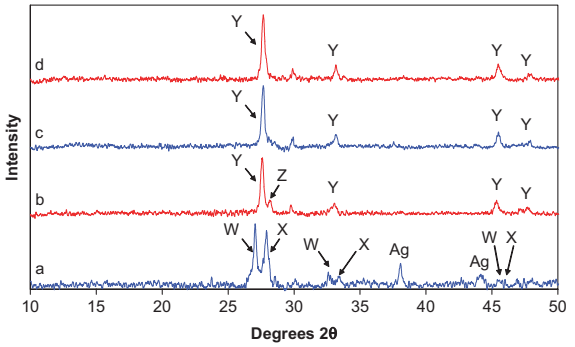

Fig. 11. XRD of heat treated samples of (a) glass 5, (b) glass 6, (c) glass 7 and (d) glass 8. Reflections from the various powellite-type molybdate phases present in these glasses are labeled 'W', 'X', 'Y' and 'Z'.

'Z' in Fig. 11(b)) at 28.26°2θ with a d-spacing of 0.316 nm. Although the phase responsible could not be identified from a single reflection, it is possible that this reflection was caused by a second powellite-type molybdate phase (as was seen in the heat treated glass 5 sample). XRD of the heat treated samples of glasses 7 and 8 (Fig. 11(c) and (d)) only showed the presence of the powellite-type molybdate phase labeled 'Y' as seen in glass 6.

These results showed that both the melting atmosphere and the quantity of Li_2O in the base glass composition had a significant effect on the crystalline phases that developed during heat treatment. In sparged glasses (glasses 1–4), the same crystalline phase developed upon heat treatment regardless of the melting atmosphere, although crystalline material was more prevalent at lower waste loadings in those glasses sparged with a reducing gas in comparison to those glasses sparged with an oxidizing gas. In the glasses which were melted in air atmospheres and stirred (glasses 5–8), two distinct crystalline phases developed upon heat treatment of the glass containing the standard quantity of Li_2O (glass 5), one distinct phase and indications of a second phase were present in a similar glass containing 3/4 the quantity of Li_2O (glass 6), and only one phase was present in the glasses containing 1/2 the quantity and no Li_2O (glasses 7 and 8 respectively). Reductions in the number of powellite-type molybdate phases developing upon heat treatment upon a reduction in the quantity of alkali in the batch have previously been noted in supercalcine ceramics by Scheetz et al. [8]. In the ceramics studied by Scheetz, a Ca–Ba–Sr molybdate phase was found, and

upon increasing the quantity of Ba and Sr in the batch, the molybdate system moved into a two phase region and a doublet was seen in the 27°2θ region of the XRD data. This was very similar to what was seen in glasses 5 and 6 in the same 27°2θ region (i.e. two molybdate phases were present at higher alkali contents). There is also evidence that the powellite-type molybdate phase labeled 'X' in Fig. 11(a) seen in the heat treated glass 5, and which is plausibly the same phase as seen in the heat treated glasses 1–4, is likely to contain Li. As the quantity of Li is reduced in the batch (in glasses 6, 7 and 8), a different powellite type molybdate (labeled 'Y' in Fig. 11(b)–(d)) that cannot contain Li (as it is present in glass 8 in which no Li_2CO_3 was present in the batch) becomes the single dominant phase. No Li was seen during the EDS analysis of the molybdate phases due to the low X-ray energies associated with this element being beyond the range of the detector.

4. Conclusions

Sparging a simulated HLW glass with a reducing atmosphere encouraged the precipitation of Ag (analogous to the heavy metals found in real HLW compositions) in the as cast state, and upon heat treatment encouraged the formation of a powellite-type molybdate phase (high in Li, Sr and lanthanides) at lower waste loadings than in glasses sparged with compressed air. In mechanically agitated melts, the quantity of Li_2O present was found to influence the number and type of powellite type molybdates formed upon heat treatment, effecting a two phase molybdate system at high levels and moving to a single phase molybdate a lower levels. However, the presence of Li_2O in the base glass composition prevented the formation of a powellite type molybdate either during the melting or annealing of the glass, a problem that did occur in those glasses devoid of Li_2O. Mo K-edge EXAFS showed that $[MoO_4]^{2-}$ tetrahedra occupied network modifier positions in the glass network in the amorphous state, and were charged balanced by a random distribution of cations in the powellite-type molybdate phase. Mo was found predominantly in the +6 oxidation state regardless of melting atmosphere.

Acknowledgements

Many thanks to Prof. F.R. Livens (of the University of Manchester) and Mr B. Billsborrow (of Darsebury Laboratories) for their help with the EXAFS work, and BNFL and the EPSRC for the funding of this work.

References

[1] I.W. Donald, B.L. Metcalfe, R.N.J. Taylor, J. Mater. Sci. 32 (1997) 5851.
[2] J.A.C. Marples, Glass Technol. 29 (1988) 230.
[3] W. Lutze, R.C. Ewing, Radioactive Wasteforms for the Future, North Holland, Amsterdam, 1988.
[4] S. Morgan, R. Hand, N. Hyatt, W. Lee, Mater. Res. Soc. Symp. Proc. 807 (2003) 151.
[5] G. Calas, M. Le Grand, L. Galoisy, D. Ghaleb, J. Nucl. Mater. 322 (2003) 15.
[6] F. Shi, J. Meng, Y. Ren, Mater. Res. Bull. 30 (1995) 1401.
[7] M. Schieber, L. Holmes, J. Appl. Phys. 35 (1964) 1004.
[8] B.E. Scheetz, W.P. Freeborn, J. Pepin, W.B. White, Mater. Res. Soc. Symp. Proc. 7 (1982) 155.